Books/Book Chapters

School of Electrical and Electronic Engineering (Former DIT)

2010

Passive All-Fiber Wavelength Measurement Systems: Performance Determination Factors

Ginu Rajan
Technological University Dublin, ginu.rajan@tudublin.ie

Yuliya Semenova
Technological University Dublin, yuliya.semenova@tudublin.ie

Agus Hatta
Technological University Dublin

See next page for additional authors

Authors

Ginu Rajan, Yuliya Semenova, Agus Hatta, and Gerald Farrell

17

Passive All-Fiber Wavelength Measurement Systems: Performance Determination Factors

Ginu Rajan, Yuliya Semenova, Agus Hatta and Gerald Farrell
Photonics Research Centre, Dublin Institute of Technology
Dublin, Ireland

1. Introduction

Passive all-fiber edge filter based devices are very often used for wavelength demodulation system for many sensors such as fiber Bragg gratings. The advantage of passive linear edge filter systems are their low cost, ease of fabrication and high measurement speed compared to active wavelength measurement systems. The accuracy and resolution of a fiber edge filter based wavelength measurement system (WMS) is determined by three main factors: the noise in the system, polarization dependence and temperature dependence of the system.

Passive edge filters used for wavelength measurements are commonly employed in a ratiometric scheme which makes the system independent of input signal power variations. A ratiometric optical wavelength measurement system's operation is perturbed by both the inherent optical noise of the input signal as well as the electrical noise due to optical-to-electrical conversion at the receivers. At the receivers, even though the measurement is performed by taking the power ratio of the signal levels, because of the uncorrelated random nature of noise, the effect of noise sources will not be eliminated and will adversely affect the system's performance. An optimization of the slope of the system considering the total noise of the system is required to achieve the best possible resolution for the widest possible wavelength range.

Since a ratiometric wavelength system contains concatenated polarization dependent loss (PDL) elements, the net effect of the PDL is different from the effect caused by individual PDL components and because of this an estimation of the range of the wavelength error is necessary to determine the accuracy of the system. PDL is an important factor determining the accuracy of fiber edge filter based WMS and needs to be minimized to improve the performance of the system. Another significant contributor that can degrade the performance of the system is temperature drift. Commonly a ratiometric WMS is calibrated and the ratio response is obtained at a fixed temperature and hence a change in temperature can alter the ratio response. It is important to know the nature of ratio variation with temperature at different wavelengths in order to evaluate and mitigate its impact on the measurement system.

This chapter focuses on these issues and their impact on the performance of a passive fiber edge filter based wavelength measurement system. It is also intended to introduce new types of passive fiber edge filters to the engineering community, which have applications in the optical sensing area where there is an increasing demand for fast wavelength measurements at lower cost. The two new edge filters introduced in this chapter are the macro-bend fiber edge filter and the Singlemode-multimode-singlemode fiber edge filter .

2. Passive all-fiber edge filters and wavelength measurement systems

Optical wavelength detection in sensing can be generally categorized into two types: passive detection schemes and active detection schemes. In passive schemes there are no power driven components involved. A passive detection scheme refers to those that do not use any electrical, mechanical or optical active devices in the optical part of the system. Most of the passive devices are linearly wavelength dependent devices such as bulk edge filters (Mille et al., 1992), biconical fiber filters (Ribeiro et al., 1996), wavelength division couplers (Davis & Kersey, 1994), gratings (Fallon et al., 1999), multimode interference couplers (Wang & Farrell, 2006) etc. In active detection schemes the measurement depends on externally powered devices and examples of these schemes include those based on tunable filters (Kersey et al., 1993) and interferometric scanning methods (Kersey et al., 1992).

2.1 Linear edge filters

The simplest way to measure the wavelength of light is to use a wavelength dependent optical filter with a linear response. This method is based on the usage of an edge filter, which has a narrow linear response range with a steep slope or a broad band filter, which has a wide range with less steep slope. In both cases, the wavelength interrogator is based on intensity measurement, i.e., the information relative to wavelength is obtained by monitoring the intensity of the light at the detector. For intensity based demodulators, the use of intensity referencing is necessary because the light intensity may fluctuate with time. This could occur not only due to a wavelength change but also due to a power fluctuation of the light source, a disturbance in the light-guiding path or the dependency of light source intensity on the wavelength. Generally, because of these factors, most of the edge filter based systems use a ratiometric scheme which renders the measurement system independent of input power fluctuations. Fig. 1 shows a schematic of a ratiometric wavelength measurement system based on an edge filter. The input light splits into two paths with one passing through the wavelength dependent filter and the other used as the reference arm. The wavelength of the input signal can be determined using the ratio of the electrical outputs of the two photo detectors, assuming a suitable calibration has taken place.
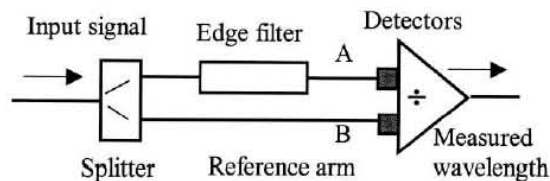

Fig. 1. Schematic of an edge filter based ratiometric wavelength measurement system

For the edge filter used in a ratiometric system, the two important parameters are its discrimination range (wavelength attenuation range) and baseline loss (transmission loss at the starting wavelength). An ideal edge filter will have a very low baseline loss and a high discrimination range. In Fig. 2 three spectral responses (A, B and C) with different discrimination ranges and baseline losses are shown and a selection of a proper response requires the knowledge of the impact of noise in the system, polarization and temperature dependences of the edge filter and their influence on the system.
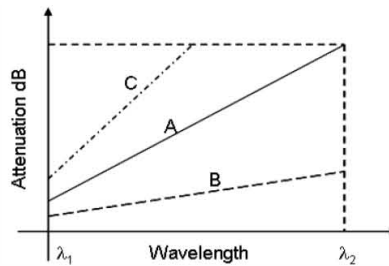

Fig. 2. Spectral response of edge filters with different discrimination range and baseline loss

The first experiment based on a ratiometric scheme was reported in 1992 and used a bulk edge filter, a commercial infrared high-pass filter (RG830), which had a linearly wavelength dependent edge in the range of 815 nm - 838 nm (Mille et al., 1992). Later the use of a biconical fiber filter was proposed as an edge filter (Ribeiro et al., 1996). This filter is made from a section of single mode depressed-cladding fiber, which consists of a contracting tapered region of decreasing fiber diameter followed by an expanding taper of increasing fiber diameter. The wavelength response of the filter is oscillatory with a large modulation depth propagating only a certain wavelengths through the fiber while heavily attenuating others. The reported filter was designed with an oscillation period of 45 nm and an extinction ratio of 8 dB. Over the range 1520 nm - 1530 nm the filter showed a near linear response with a slope of 0.5 dB/nm. Another type of passive wavelength filter is the one based on a wavelength division multiplexing coupler which was first proposed by Mille et. al. and demonstrated by Davis and Kersey. In this scheme the WDM coupler has a linear and opposite change in coupling ratios between the input and two output ports. Another reported edge filter is the one based on long period gratings (LPG) (Fallon et al., 1998). An LPG utilizes the spectral rejection profile to convert wavelength into intensity encoded information. The latest addition to linear fiber edge filters are fiber bend loss filters and single-mode-multimode fiber filters which are explained in the section below.

2.2 A fiber bend loss edge filter
One of the recent additions to the range of available fiber edge filters are bend fiber filters (Wang et al., 2006). This filter comprises of multiple macro bends of standard singlemode fiber (eg. SMF28) coated with an absorption layer. The filter can be made further compact by using a single turn of a buffer stripped bend sensitive fiber (eg. 1060XP) with an applied absorption coating (Wang et al., 2007). The cross sections of both the fiber filters are shown in Fig 3(a) and Fig 3(b) respectively. Prototypes of the filters are shown in Fig 3(c) and Fig 3(d) respectively. To use a macro-bend fiber as an edge filter for wavelength measurement,

the optimal design of the bend radius and surface processing methods are required to achieve a linear transmission response with wavelength.

(a)   (b)

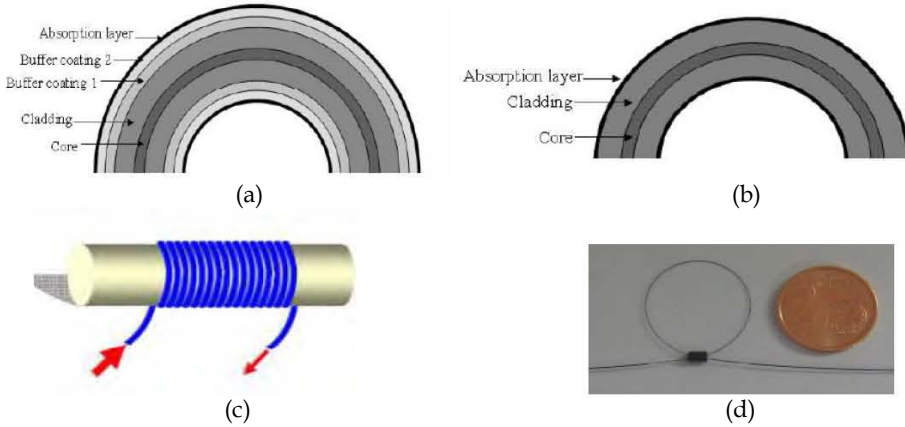(c)   (d)

Fig. 3. Cross sections of SMF28 (a& c) and 1060XP (b& d) bend fiber edge filters and their prototypes

It is known that for an optical waveguide with an infinite cladding the bend loss will increase as the bend radius decreases. However, a practical fiber contains one or two coating layers outside the cladding to offer mechanical protection. Because of the reflection of the radiated field at the interface between the cladding layer and the coating layer, so-called whispering gallery modes (WGM) are created and the fiber shows significantly different bend loss characteristics as compared to the simple case of an infinite cladding. The theoretical and experimental investigations (Wang et al., 2005), which considered the bend loss in SMF28 standard single-mode fiber, taking into account two coating layers, show that the bend loss is in the measurable range (40 dB) of photo detectors for bend radii in the range of 9.5 mm - 11 mm. To use the macro-bend loss fiber as an edge filter it is also
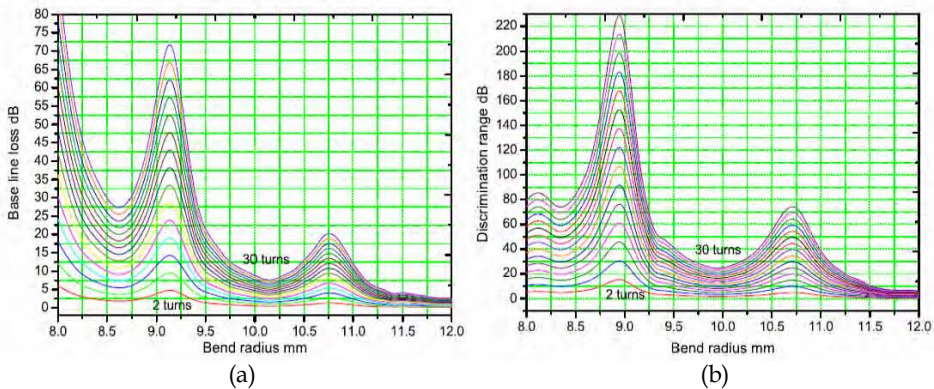

(a)   (b)

Fig. 4. (a) Baseline loss and (b) discrimination range for filters with differnent numbers of bend turns and bend radii

important to achieve a linear wavelength response and an acceptable discrimination range. Fig. 4(a) and Fig. 4(b) show the predicted baseline loss (at 1500 nm) and discrimination range (from 1500-1600 nm) for different fiber filters. From this response one can determine the baseline attenuation and the discrimination range of the filter. By changing the bending length or by increasing or decreasing the number of bend turns, at a fixed bend radius baseline attenuation and discrimination range can be varied.

As mentioned earlier in the case of a bend fiber, when the radiated field escapes from the cladding layer, some of the radiated field is reflected back and forms whispering- gallery modes, while the rest penetrates into the coating layers. Most of the radiated field reaching the coating is absorbed or scattered in the coating layers, but a small amount of the radiated field reaches the fiber surface. Because of the strong reflection at the interface between the outer coating layer and the air, the field reflected back toward the core affects propagation in the bending fiber, resulting in a transmission spectrum which displays non-linear variations. To remove such variations and to make the bending fiber suitable as an edge filter, one has to eliminate the back reflections at the coating-air interface. One simple method to remove the reflections at the air boundary is to apply an absorption layer which absorbs light in the wavelength range of 1500 nm – 1600 nm. The simplest example of such a coating is a black pigment ink (Indian ink) or a carbon paste. Indian ink is generally considered as a good optical absorber (Mourant et al., 1997). The transmission response of the filter before and after applying the absorption layer is shown in Fig. 5(a) and Fig. 5(b) respectively for filters with different bend radii. It can be seen that the transmission responses in Fig. 5(b) are much smoother after applying the absorption layer and quasi linear in comparison to those in Fig. 5(a), thus allowing a macro-bend fiber to be reliably used as an edge filter.
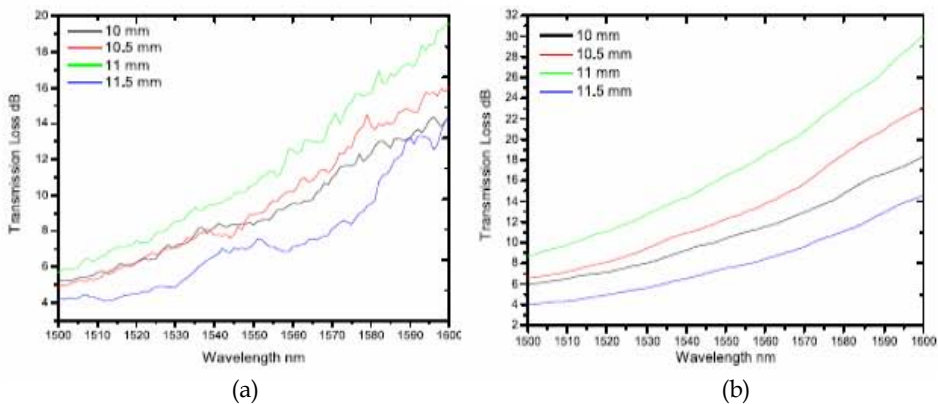

(a)   (b)

Fig. 5. Transmission response of the fiber filter (a) before and (b) after absoprtion coating

2.3 A singlemode-multimode-singlemode (SMS) fiber edge filter

Another recently inducted fiber edge filter is the singlemode-multimode-singlemode fiber filter (Wang et al., 2008). It is formed by splicing a step-index multimode fiber (MMF) between two standard singlemode fibers (SMF). An SMS edge filter structure is shown in Fig. 6. The operating

mechanism for this edge filter can be described as follows: the light field propagating along the input SMF enters the MMF section and excites a number of guided modes in the MMF. Interference between the different modes occurs while the light field propagates through the MMF section. By choosing a suitable length for the MMF section, the light is coupled into the output SMF in a wavelength dependent manner due to interference. The input-to-output transmission loss is expected to increase/decrease monotonically, as the wavelength of the propagating light increases in a certain wavelength range.
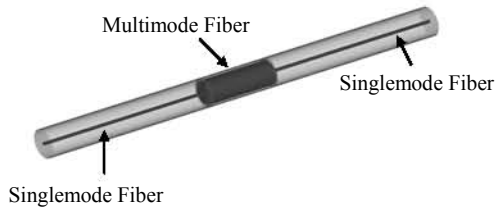

Fig. 6. Schematic of an SMS edge filter

A modal propagation analysis for linearly polarized (LP) modes can be used to investigate light propagation in the SMS fiber structure. To design the SMS based edge filter, the MMF length needs to be accurately determined. At a re-imaging distance (the transmission loss will reach a peak at a self image of the input) the filter is highly wavelength dependent. If re-coupling of light into the SMF takes place at the re-imaging distance, then the SMS structure operates as a band-pass filter as shown in Fig. 7. However for the purpose of designing an edge filter, the band-pass response can be considered as two edge-type responses, on the either side of a center wavelength. Consequently the device can behave as an edge filter with either a positive or a negative slope for a selected wavelength range.
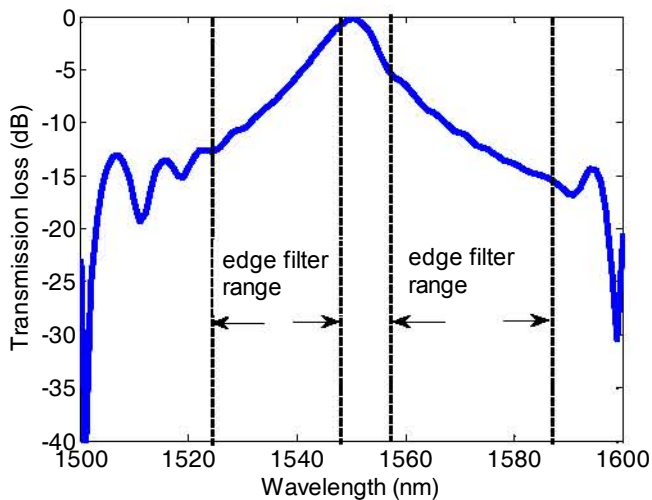

Fig. 7. Typical spectral response of an SMS fiber filter

3. Factors determining the performance of a linear edge filter based WMS

Precision, accuracy and resolution are extremely important for wavelength measurements involved in multi-channel dense wavelength division multiplexing (DWDM) optical communication systems and fiber Bragg grating based optical sensing systems (Hill & Meltz, 1997). The core component of a passive wavelength measurement system for such applications is a linear edge filter (Zhao & Liao, 2004). Therefore it is important to study the factors that influence the performance accuracy of such a system.

The three main factors that determine the performance of a linear edge filter based wavelength measurement system are:

1. Noise in the receiver system and the signal-to-noise ratio (SNR) of the source.
2. Polarization dependency of the components involved in the system.
3. Temperature dependence of the components involved in the system.

4. Modelling and analysis of impact of noise on the resolution and accuracy of an edge filter based WMS

Many of the interrogation schemes employed in optical sensing are based on a ratiometric wavelength approach which makes the system independent of input signal power variations. However a ratiometric optical wavelength measurement system's operation is perturbed by both the inherent optical noise in the input signal as well as the electrical noise due to optical-to-electrical conversion at the receivers. At the receivers, even though the measurement is performed by taking the power ratio of the signal levels, because of the uncorrelated random nature of receiver noise, the effect of noise sources will not be eliminated, but will affect the system's performance adversely.

4.1 Influence of SNR of the source on the ratio response of a WMS
In practice a narrow-band input to the wavelength measurement system with a center wavelength λ_0 could originate from a tunable laser source or a reflection from a fiber Bragg grating. Such an input signal can be approximated as a Gaussian function with a spectral
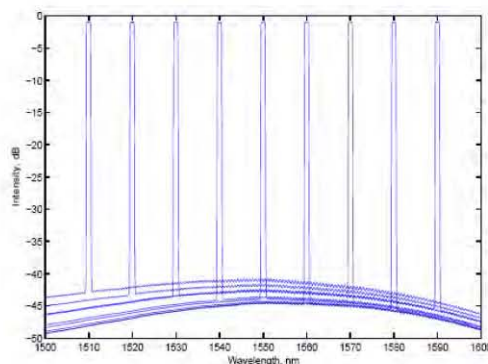

Fig. 8. Intensity distribution of a typical tunable laser source in the wavelength region 1500 nm to 1600 nm.

width $\Delta\lambda$ and center wavelength λ_0. An input signal from any source generally has a limited

SNR, which means that there is measurable power even far from the center wavelength of the spectrum. For example in Fig. 8, the typical spectral distributions of the output intensity from a tunable laser at different central wavelengths, measured by an optical spectral analyzer in a wavelength range from 1500 nm - 1600 nm are shown. From these measured spectral distributions it can be seen that for this tunable laser the source spontaneous emission ratio is >40 dB and has different values for different output center wavelengths. To take account of the SNR, the output spectral response of the source (Xu et al, 1996) can be described as (the power at the peak wavelength is assumed as 0 dBm),

$$10\log_{10}\left[I_{\lambda_0}(\lambda)\right] = \begin{cases} 10\log_{10}\left[\exp(-4\ln 2\dfrac{(\lambda-\lambda_0)^2}{\Delta\lambda_0^{~2}}\right], & \left|\lambda-\lambda_0\right| \le \Omega \\ -S(\lambda) + Rand.Rs, & \left|\lambda-\lambda_0\right| > \Omega \end{cases} \tag{1}$$

where S is the SNR of the source. To describe the random fluctuations in the noise floor of the optical source, the term $Rand.Rs$ is used, where $Rand$ is a random number (between +0.5 and -0.5) and Rs is a parameter in dB which dictates the peak fluctuation in the SNR and is dependent on the nature of the source. Ω is a parameter which is determined by the noise level and can be found for a source with a given SNR from the relation:

$$10\log_{10}\left[\exp\left(-4\ln 2\frac{\Omega^2}{\Delta\lambda_0^{~2}}\right)\right] = -S \tag{2}$$

For real-world wavelength measurements there is always a possibility that the input signal's SNR may change from that used in the initial calibration. This can happen, for example, when the system is switched to a different source and in such cases the measured wavelength will have an error as the calibration is done for a different SNR. Fig. 9(a) shows
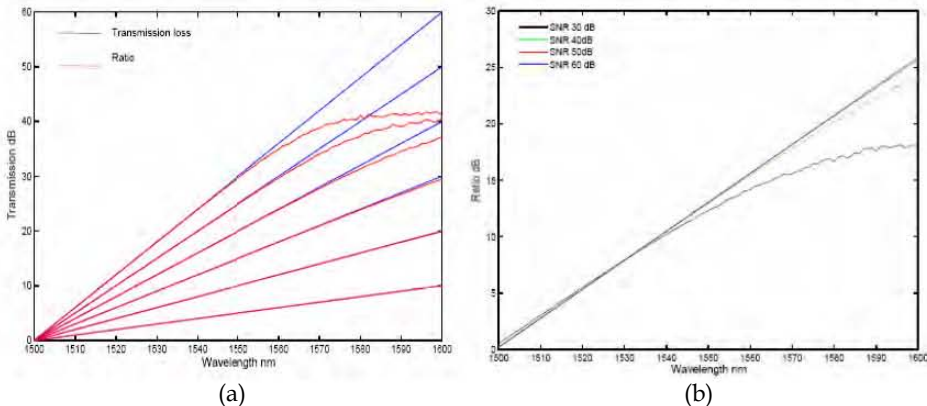

(a)   (b)

Fig. 9. (a) Trasmission responses of edge filters of different slope at a fixed SNR (50 dB) (b) Transmission response of an edge filter with a fixed slope (0.25 dB/nm) at different SNRs

the ratio response of a system for edge filters of different slope at a fixed SNR while in Fig.

9(b) the ratio response of an edge filter at a fixed slope at different SNRs are shown. From the figure it can be seen that a decrease in SNR of the source produces a great level of non-linearity in the discrimination characteristic, in particular for low values of SNR, the slope of the edge filter is reduced significantly at longer wavelengths, impairing accuracy and resolution. For any edge filter based ratiometric wavelength measurement system, source SNR is an important factor that needs to be considered as the limited SNR of the optical source affects the system by limiting the slope of the filter and also the measurable wavelength range (Rajan et al., 2007).

4.2 Noise mechanisms in an optical receiver

An understanding of the origin of receiver noise is required for a receiver performance to be accurately characterized. The amount of noise present in a receiver will be the primary factor that determines the receiver sensitivity. Fig. 10 shows a simple but adequate noise model of a trans-impedance optical receiver (Motechenbacher & Connelly, 1993), where I_{th}, I_{sh}, I_{amp} and e_{amp} are the thermal noise, shot noise, amplifier current noise and amplifier voltage noise respectively. C_f and C_d are the feedback and photodiode capacitance respectively. In addition, in optical sensing applications, it is very likely that every receiver has an analog-to-digital converter (ADC) associated with it. So the receiver system noise will also contain the quantization noise from the ADC. For simplicity the main noise mechanisms considered in this analysis are (a) shot noise of the photodiode (b) thermal noise and (c) quantization noise. If a low noise pre-amplifier is used which has a very low I_{amp} (in the order of fA) and e_{amp} (15 nv/$\sqrt{Hz}$, f=1 kHz, shunt resistance=100 Ω) then the effect of amplifier noise can be neglected.
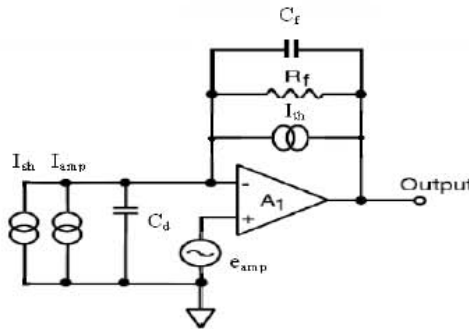

Fig. 10. Noise equivalent circuit of a trans-impedance amplifier.

Shot noise: In a photodiode the conversion of photons to charge carriers is a random process and the noise generated in this process is called shot noise. Because shot noise is associated with current flow, it is naturally modeled as a current-noise source in parallel with the photodiode, whose mean square value is given as

$$I^2{}_{sh} = 2eI_{ph}B \qquad (3)$$

where I_{ph} represents the average photon generated current flowing through the photodiode, B is the post-conversion electrical bandwidth of the system and e is the elementary charge.

When a photodiode is used together with a trans-impedance pre-amplifier, the shot noise produced in the photodiode is amplified together with the original signal. If A_{sig} is the amplification factor of the pre-amplifier, the rms shot noise voltage will be

$$e_{sh} = \sqrt{2eI_{ph}B}.A_{sig} \qquad (4)$$

Thermal noise: Thermal noise is a result of thermally induced random fluctuations in the number of charge carriers in an electrical resistance element. Carriers are in random motion in all resistances at a temperature higher than absolute zero. The amount of motion is a direct function of the absolute temperature of the resistance. Nyquist showed that the open circuit rms voltage produced by a resistance R is given by

$$e_{th} = \sqrt{4KTR_f B} \qquad (5)$$

where K is the Boltzmann's constant, T is the absolute temperature in Kelvin and B is the electrical system bandwidth. In the case of a trans-impedance amplifier front end the main source of thermal noise is the feed back resistor R_f.

Quantization noise: Quantization noise is a noise error introduced by quantization in the analog-to-digital converter used to convert an analog signal to a digital signal. A digital signal representation of an analog signal involves discrete levels and thus has an accuracy that depends on the quantization resolution or number of bits used to represent samples in the analog to digital process. Therefore, when converting a continuous analog level into a discrete digital level, the actual analog value must be approximated as a digital value. The error arising during this conversion is called quantization error. Quantization error can be treated as random noise added to the converted signal and is referred to as quantization noise.

4.3 Noise model of a ratiometric wavelength measurement system
The ultimate precision and resolution of wavelength measurement is determined by the electrical noise in the receiver and the signal-to-noise ratio of the input optical signal. As a starting point to determine the effects noise on a ratiometric system a basic noise source representation of the system is considered (Rajan et al., 2008) and is presented in Fig. 11.
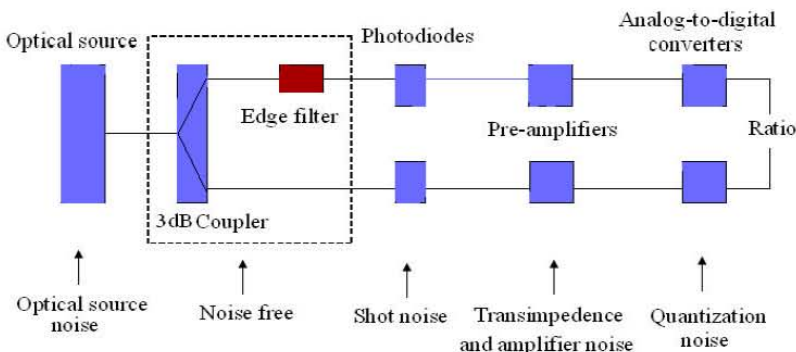

Fig. 11. Noise model of an edge filter based ratiometric system.

Since the different noise mechanisms are statistically independent the total mean square electrical noise that contributes to each arm of the system can be expressed as the sum of the

individual mean square noises. Assuming a low noise pre-amplifier, the amplifier noise can be neglected. Thus the total rms noise voltage can be expressed as:

$$e_o = (e_{sh}^2 + e_{th}^2 + e_{adc}^2)^{1/2} \qquad (6)$$

The calculated total rms noise voltage from all sources for a wavelength range from 1500 nm to 1600 nm for the receivers connected to both the reference arm and edge filter arm for different filters are shown in Fig. 12. At higher wavelengths the main noise contribution is the quantization noise of the analog-to-digital converter.
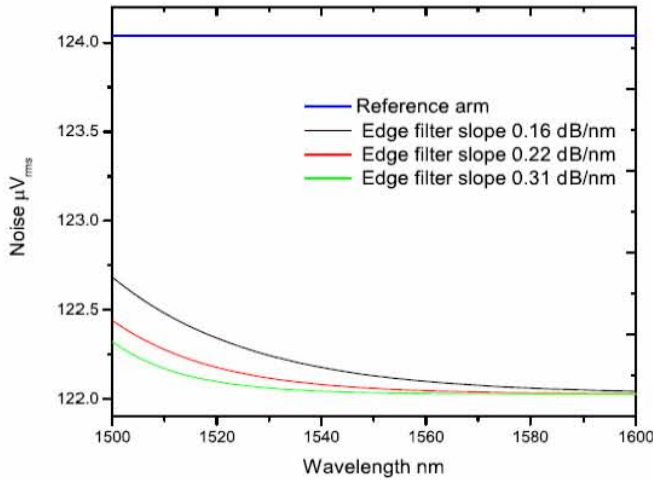

Fig. 12. Total rms noise of the receivers connected to reference arm and edge filter arms with filters of different slope.

4.4 Ratio Response of the system considering noise effects

In the previous section the ratiometric system was analyzed in the context of the limited signal-to-noise ratio of the input signal and it was shown that for a given measurable wavelength range, the slope of the edge filter is effectively limited due to the noise level of the input signal. To take account of the noise of the receivers connected to the reference and the edge filter arms, together with the signal-to-noise ratio of the input signal, the ratio of the system at a wavelength λ_0 can be expressed as

$$R(\lambda_0) = -10\log_{10}\left[\frac{\int I_{\lambda 0}(\lambda)T_f(\lambda)d\lambda + Grand_{e\lambda 0}}{\int I_{\lambda 0}(\lambda)d\lambda + Grand_r}\right] \qquad (7)$$

T_f is the transmission response of the edge filter which in the simple case is a linear function within a wavelength range (λ_1, λ_2). Gaussian statistics is used to model the electrical noise. $Grand_e$ and $Grand_r$ are Gaussian random numbers used to represent the receiver's noise with a mean value 0 and standard deviation equal to the rms noise of the receivers connected to

the edge filter and reference arms respectively and are uncorrelated to each other. As the shot noise of the receiver connected to edge filter is a function of wavelength it makes $Grand_e$ also wavelength dependent.

To understand the separate effects of optical noise and receiver noise on the ratio fluctuation, the ratio fluctuation is calculated for the system with different edge filters in the presence of receiver noise by assuming the source SNR is infinite (100 dB). Then to calculate the ratio fluctuation that arises due to the noise of the input signal, the receivers are assumed to be noise free. The ratio fluctuations in both cases are shown in Fig. 13(a) and Fig. 13(b) respectively. For a system with an infinite source SNR the ratio fluctuation is caused due to the receiver noise and is very low at lower wavelengths as shown in Fig 13(a). For an ideal receiver with zero noise the ratio fluctuation is due to the source's noise and changes as the SNR of the source changes as shown in Fig. 13(b).

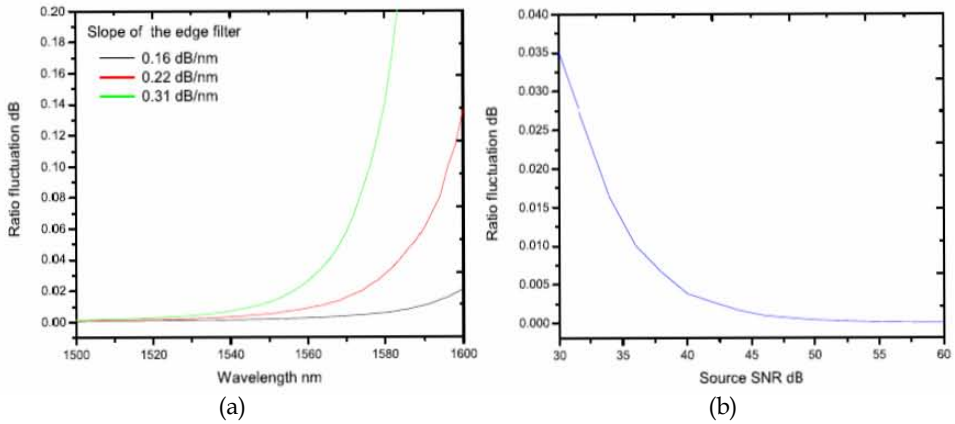(a)   (b)

Fig. 13. (a) Ratio fluctuation of the system arises from the receiver noise (b) ratio fluctuation arises from the limited SNR of the source.

In practice all optical sources have a limited signal-to-noise ratio and the net ratio fluctuation of the system is determined by the combined effect of optical noise and the receiver noise. Taking in account both a limited source SNR and the presence of receiver noise, the net ratio fluctuation can be calculated using equation (7). Fig. 14(a) shows the total ratio fluctuation of the system with different edge filters and with input signals with different SNRs. Fig. 14(b) shows a comparison of the modelled ratio fluctuation and the experimentally measured ratio fluctuation for edge filters of different slope at a fixed SNR. From the figures it can be seen that the ratio fluctuation is high at longer wavelengths which is the effect of the receiver noise and also the level of noise fluctuation increases irrespective of wavelength when the SNR of the input signal changes. Thus in the design of a ratiometric system it is important to consider the inaccuracy in measurement due to any changes in the SNR of the source and the noise in the receiver system. Ultimately to maintain accuracy it may be necessary to ensure that the SNR of the input signal is the same as that used during calibration.
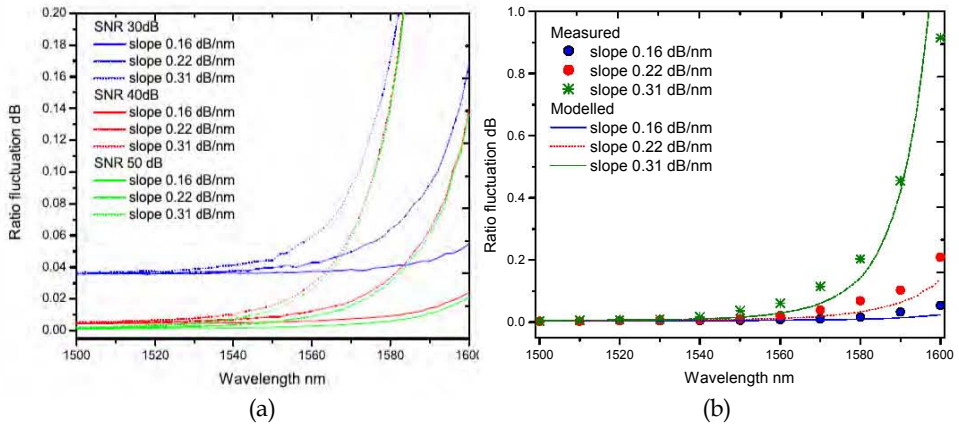
Fig. 14. (a) Ratio fluctuation of the system for different optical SNR and (b) for different edge filters of different slopes at a fixed SNR

4.5 Influence of Noise on the Resolution of the System

From the Fig. 14 it is seen that the ratio fluctuation increases as the wavelength increases, which limits the wavelength resolution of the system in addition to the wavelength range. In any measurement system perturbed by noise, the resolvable step change should be higher than the peak-to-peak fluctuation of the parameter being measured. In the case of ratiometric wavelength measurement system the minimum reliable detectable ratio variation corresponding to a wavelength shift is assumed equal to the peak-to-peak ratio fluctuation and can be expressed as

$$\Delta R(\lambda_0)_{min} = [R(\lambda_0)]_{p-p} \qquad (8)$$

For a system of known slope m_r the wavelength resolution can be determined from the ratio fluctuation, which is given as

$$resolution = [R(\lambda_0)]_{p-p} \Big/ m_r \qquad (9)$$

Assuming a linear slope the estimated wavelength resolution for systems containing different edge filters (slopes of 0.16dB/nm, 0.22 dB/nm and 0.31 dB/nm) are shown in Fig. 15(a), Fig. 15(b), Fig. 15(c) respectively at different wavelengths (different receiver noise levels) and for different optical source SNRs. It is clear that a 10 pm resolution is possible for all systems below 1520 nm if the SNR of the source is above 50 dB. When the SNR drops, for a system with edge filter having a higher slope, a high resolution is achieved only at lower wavelengths. For example, for the systems with slopes of 0.16 dB/nm, 0.22 dB/nm and 0.31 dB/nm a 10 pm resolution can be achieved in the range of 36 nm, 22 nm, 16 nm respectively starting from 1500 nm in the presence of receiver noise and an input signal SNR of 50 dB. Thus the slope of the filter used within a system in the presence of receiver noise and optical noise depends on the required resolution and wavelength range. High

resolution in a very narrow wavelength range can be obtained with an edge filter with a higher slope, while for a wide wavelength range a reasonable resolution can be obtained with an edge filter of lower slope.

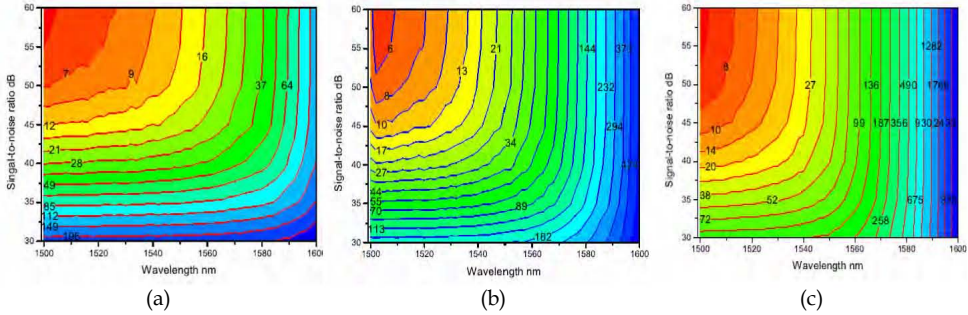<center>(a)   (b)   (c)</center>

Fig. 15. Contour plots of achievable resolution for system contains edge filters of slope (a) 0.16 dB/nm (b) 0.22 dB/nm (c) 0.31 dB/nm

For further illustration, experimentally measured ratio variations for a wavelength step of 20 pm from 1550 nm are shown in Fig. 16 (a), Fig. 16 (b), Fig. 16 (c) for the systems with three different edge filters. From the figure it is seen that a wavelength change can be resolved more readily for the system with an edge filter of 10 turns than by systems that use edge filters with a larger numbers of turns (and thus higher slopes). This confirms the assertion arising from the model that increasing the slope of filter itself will not improve the resolution. Also it is not possible to achieve the same resolution throughout the wavelength range and for a system with a given edge filter a higher resolution will always be achieved at lower wavelengths.
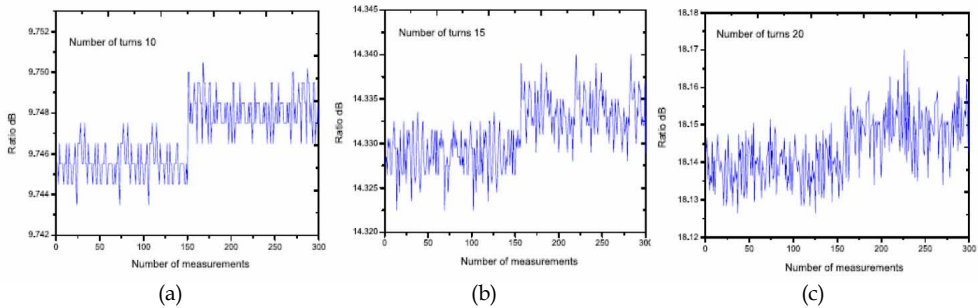

<center>(a)   (b)   (c)</center>

Fig. 16. Ratio variation for 20 pm wavelength step at 1550 nm for the systems with edge filters (a) 10 turns (b) 15 turns (c) 20 turns.

5. Polarization analysis of an edge filter based WMS

A typical ratiometric detection system consists of a 3 dB coupler and an edge filter, both of which are polarization sensitive devices. If the system contains more than one polarization sensitive component connected by standard optical fibers, its global PDL may fluctuate and hence the measured ratio also fluctuates. The fluctuation in the ratio will have an impact on the performance accuracy of the system. The fluctuation arises because the state of polarization of the input light to the system may vary randomly, for example because of stress variations in the connecting fibres or a change of source etc. A system calibrated at a particular input polarization state gives errors as the power attenuation will be different because of the polarization dependency of the elements.

Prior to the introduction of systems which demand very high wavelength accuracy (such as DWDM), the role of PDL in a ratiometric system was not considered important. DWDM systems require an accurate control of each channel's wavelength, e.g., the allowable maximal frequency deviation for 25 GHz channel spacing (2.5Gbit/s) is 4-5 GHz, i.e., 0.032-0.04 nm according to the ITU-T Recommendation G.652. In a system where high accuracy is needed errors from all sources must be calculated in order to estimate the accuracy and resolution and in such a case the error from the PDL is important (Rajan et al., 2008).

The PDL of an optical component is commonly defined as the difference between the maximum and the minimum insertion losses for all the possible states of polarization. If T_{min} and T_{max} are the minimum and maximum transmission coefficients of an optical element, then PDL can be expressed as

$$PDL_{dB} = 10\log\left(T_{max} / T_{min}\right) \tag{10}$$

5.1 Polarization sensitivity of a 3 dB coupler

It is very well known that a 3 dB coupler is a polarization sensitive device. The common fabrication technique for a coupler is the fused-fiber method which involves twisting, melting, and pulling two single-mode fibers so they are fused together over a uniform length section. During fabrication a deviation of the coupler geometry from a circular symmetry to the elliptical shape in the fused tapered region can occur and this changes the coupling characteristics of polarization states and leads to birefringence, which makes the coupler polarization sensitive and therefore a device exhibiting PDL (Wu & Chang, 1995). The polarization sensitivity of a 3 dB coupler mainly depends on the geometrical structure parameters and the degree of fusion (Wu, 1999). The PDL of any device is commonly characterized at a specific wavelength. But because of the wavelength dependency of PDL and especially for wavelength measurements, the PDL of the components has to be considered over the whole range of wavelengths from 1500 - 1600 nm. Typical commercially available 2x2 fused couplers have a PDL of 0.1 - 0.15 dB at the central wavelength, but the value does vary with wavelength as shown in Fig. 17.
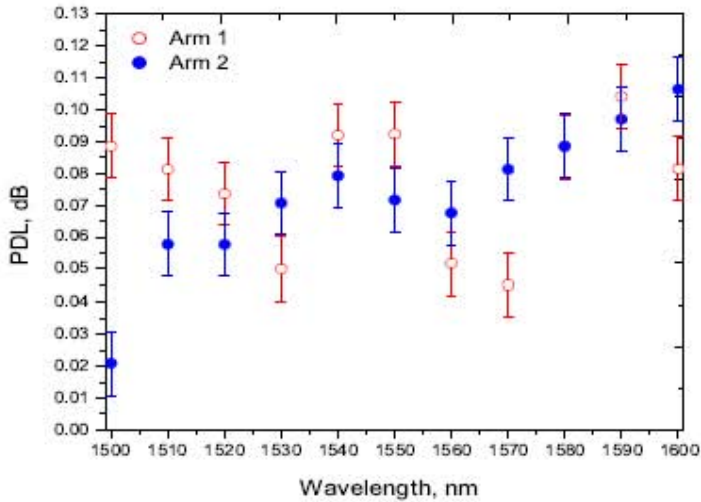
Fig. 17. Measured PDL of the arms of a 3dB coupler for a wavelength range 1500-1600 nm

5.2 Polarization sensitivity of edge filters

In this section the polarization sensitivity of macro-bend fiber filter and SMS fiber filter are explained. There are a couple of reasons which underpin the polarization sensitivity of a bent fiber. The state of polarization of light propagating along a single-mode fiber can be influenced by perturbations, such as bending and twisting. In a macro-bend fiber filter it can originate from the anisotropic nature of the refractive index caused by the bending stress. Single-mode fibers with nominal circular symmetry about the fiber axis are in fact bimodal and they can propagate two nearly degenerate modes with orthogonal polarizations, the TE and TM modes. The bend induced mechanical stress can induce birefringence by changing the modes of polarization. In the case of a standard single-mode fiber such as SMF28, the stress induced refractive index variation is very small. As a result, the bend induced birefringence will have only a small impact on the polarization modes propagating along the fiber. A practical single-mode fiber consists of a core, a cladding and a polymer coating layer which offers mechanical protection. The difference in the refractive index between the polymer coating layer and the cladding layer is much higher as compared to that between the cladding and core. The reflectance of the radiated field occurring at the interface between the coating layer and cladding layer is believed to be different for different polarization states. This can lead to polarization dependence of the bend loss, which originates because of the coupling between the reflected radiated field and the guided fundamental mode (Wang et al., 2007). Thus, the main contributor to the polarization sensitivity of a bend single-mode fiber is the polymer coating.
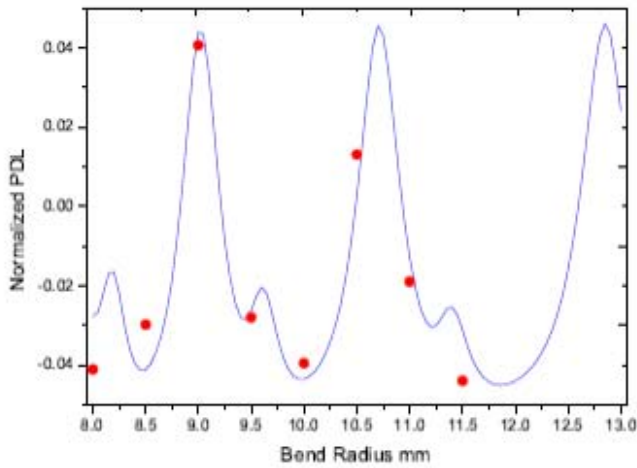
Fig. 18. Normalized PDL of 10 turns of SMF28, simulated and measured at 1550 nm

The theoretical model of polarization sensitivity of bend fiber shows that the TE and TM modes propagating along the fiber experience different values of bend losses. Similar to the bend loss behaviour of a single-mode fiber (Fig. 4) the absolute PDL does not increase monotonically with the bend radius. The normalized polarization dependence has a quasi-periodical characteristic with bending radius and this quasi-periodical behaviour is very close to that of the bend loss vs. bending radius of a standard single mode fiber. Since the bend loss varies with wavelength, the PDL also changes with wavelength. The normalized PDL for 10 turns of SMF28 for different bend radii is shown in Fig. 18.
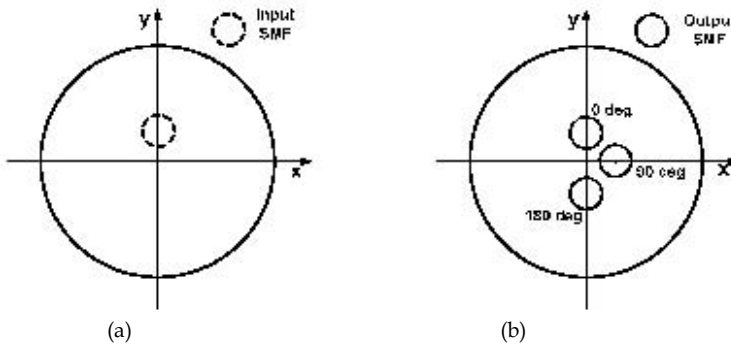

(a)   (b)

Fig. 19. Interfaces of input/output SMF core to the MMF core (a) position of input SMF core, and (b) position of output SMF core.

The main source of PDL in a SMS edge filter originates from the lateral core offset that occurs during the splicing between the singlemode fiber and the multimode fiber, i.e. the input/output SMFs may have lateral core offsets relative to the centre of the MMF core.
In addition the two lateral core offsets at each end of the MMF may also have a different orientation relative to each other which can be referred to as a rotational offset. In order to

analyze the PDL of a SMS fibre structure, a means to precisely describe lateral and rotational offsets is needed. Fig. 19(a) and Fig. 19(b) show the interfaces between the input SMF and the MMF section cores and the MMF section and the output SMF cores, respectively.

Assuming some lateral core offset of the input SMF is as in Fig 19(a), the field profile at the output end of the MMF section depends on the input field polarization state of the quasi TE mode (x-directed) or quasi TM mode (y-directed). In turn, the transmission loss for each mode depends on the overlap between the field profile at the output end of the MMF section and the eigen-mode profile of the output SMF. Thus the PDL can be calculated from the difference in the transmission loss between the quasi TE and quasi TM modes in dB using the equation;

$$PDL = \left| Ls_{TE} - Ls_{TM} \right| \tag{11}$$

The PDL of the SMS fiber edge filter for different lateral and rotational offsets is shown in Fig. 20. Generally, a larger lateral core offset induces a higher PDL.
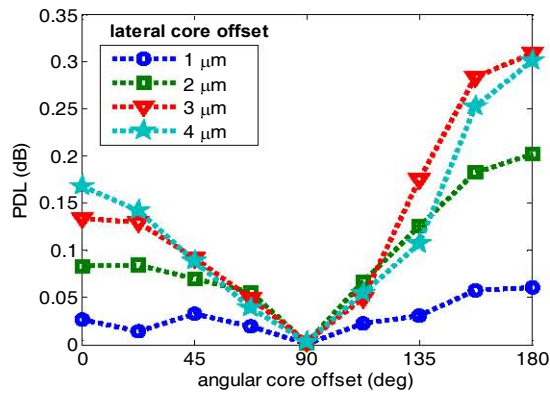

Fig. 20. PDL of the SMS fiber filter for several lateral core offsets at the rotational core offset from 0 to 180⁰.

5.3 Theoretical model to estimate the range of PDL and ratio fluctuation

As mentioned above, in a fiber edge filter based ratiometric wavelength measurement system, the PDL components are the edge filter itself and the 3 dB coupler. The total PDL of the system is not simply the sum of the contribution of each PDL element. If the polarization sensitive axis of the 3 dB coupler and the fiber filter are not aligned with each other, the resulting PDL depends on the relative orientation of the PDL axes at each connection. In an all-fiber ratiometric configuration the PDL will fluctuate in the filter arm as it effectively contains two PDL elements. The total attenuation ratio fluctuation of the system depends on the PDL of both the filter arm and the reference arm. The edge filter considered in this analysis is a bend fiber edge filter.

The general expression for PDL of any optical component is given by Equation (10). But a more convenient approach is to express the PDL as a 3-dimensional vector $\vec{\Gamma}$ (Gisin, 1995) of length Γ as

$$\Gamma = \frac{T_{\max} - T_{\min}}{T_{\max} + T_{\min}} \tag{12}$$

If Γ_{3dB} and Γ_{bend} are the PDL of the 3 dB coupler and the fiber filter, the net PDL of the filter arm can be expressed as (Almari et al., 1998)

$$\vec{\Gamma}_{3dBbend} = \frac{\sqrt{1 - \Gamma_{bend}^2}}{1 + \vec{\Gamma}_{3dB}\vec{\Gamma}_{bend}} \vec{\Gamma}_{3dB} + \frac{1 + \vec{\Gamma}_{3dB}\vec{\Gamma}_{bend}\left(1 - \sqrt{1 - \Gamma_{bend}^2}\right)/\Gamma_{bend}^2}{1 + \vec{\Gamma}_{3dB}\vec{\Gamma}_{bend}} \vec{\Gamma}_{bend} \tag{13}$$

The maximum value of the PDL will occur when Γ_{3dB} and Γ_{bend} are parallel and minimum occurs when they are anti parallel. The maximum and minimum global PDL of the fiber filter arm (Γ_{Gmax} and Γ_{Gmin}) can thus be expressed as

$$\Gamma_{G\max} = \frac{\Gamma_{3dB} + \Gamma_{bend}}{1 + \Gamma_{3dB}\Gamma_{bend}} \qquad \text{and} \qquad \Gamma_{G\min} = \frac{\left|\Gamma_{3dB} - \Gamma_{bend}\right|}{1 - \Gamma_{3dB}\Gamma_{bend}} \tag{14}$$

Using these equations the range of PDL of the filter arm can be predicted and together with the PDL of the reference arm of the system the ratio error of the system can be estimated. The maximum variation in the ratio from the calibrated value occurs when one arm gives the maximum attenuation and the other gives the minimum attenuation for a given state of polarization. Since the photodiodes measure the integral power over the wavelength range, by knowing the maximum and minimum power at the arms of the system when the polarization state changes, the maximum possible polarization dependent change in ratio of the system for any wavelength can be obtained and is expressed as

$$\Delta R_{\max} = 10\log_{10}\left[\frac{\int P_{1\max}(\lambda)I_{\lambda 0}(\lambda)d\lambda}{\int P_{2\min}(\lambda)I_{\lambda 0}(\lambda)d\lambda}\right] - 10\log_{10}\left[\frac{\int P_{1\min}(\lambda)I_{\lambda 0}(\lambda)d\lambda}{\int P_{2\max}(\lambda)I_{\lambda 0}(\lambda)d\lambda}\right] \tag{15}$$

where P_{1max} and P_{2min} are the maximum and minimum output powers of the filter arm when the polarization state changes and P_{2max} and P_{2min} are that of the reference arm. $I_{\lambda 0}$ is the narrow band input signal with a central wavelength λ_0 which could be from tunable laser source. By knowing the variation in the ratio the corresponding wavelength variation can be calculated.

5.4 Ratio and wavelength error due to PDL

The ratio responses of an edge filter based ratiometric system at different polarization states are shown in Fig. 21. The ratio response for polarization state A is the calibrated response, while the response curves for the two other states B and C show the variation in ratio response from the calibrated response as the polarization state changes. The experimental arrangement to measure the polarization induced errors is shown in Fig. 22. A manual fiber polarization controller is used to change the polarization state of the input signal from a tunable laser source. The polarization controller allows for the complete control of the output polarization state and the output power varies with the change in polarization states for a particular wavelength. It is assumed that the fiber polarization controller covers all the possible polarization states at a fixed wavelength.
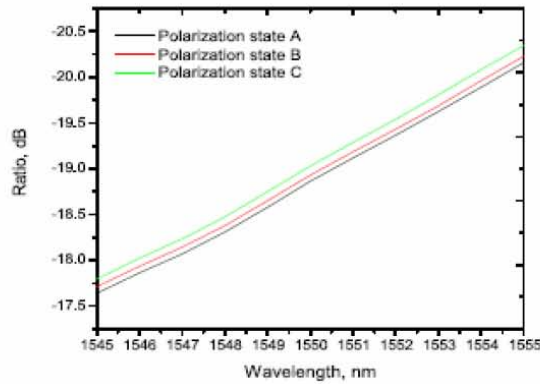
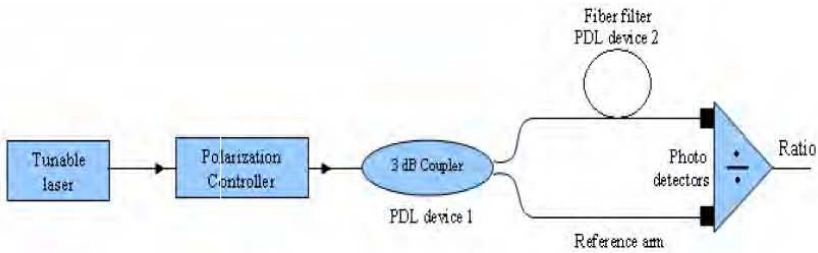Fig. 21. Ratio response of the system at different polarization states

Fig. 22. Experimental arragement to study the impact of PDL on wavelength measurements

Estimation of the maximum variation in the measured wavelength is important as we can determine the system's worst case performance. The maximum and minimum values of the fluctuation of PDL of the filter arm due to the 3 dB coupler and the fiber filter can be calculated using Equation (14). A comparison of the estimated maximum and minimum of the PDL of the filter arm with the measured PDL of the filter arm is shown in Fig. 23.
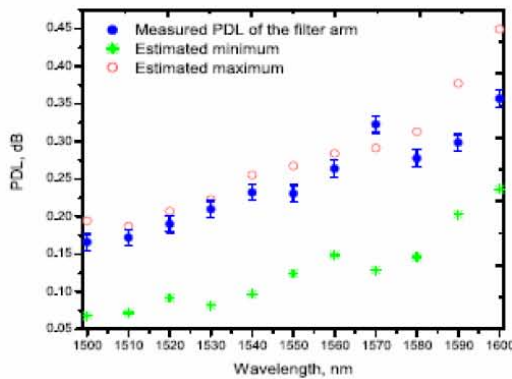

Fig. 23. Maximum and minimum PDL of the fiber filter arm and its comparison with the measured PDL.

For a ratiometric system both of the arms contribute to the total ratio variation. The PDL of the reference arm and filter arm obtained from the experiment provides the maximum and minimum power levels of each arm. Based on that, a numerical simulation can be carried out to find the maximum ratio variation and can be estimated using Equation (15). The estimated variation in ratio and wavelength of the system and its comparison with the measured versions are shown in Fig. 24(a) and Fig. 24(b) respectively. To estimate the wavelength error, the local slope of the ratio spectrum is used. The wavelength error, which is a consequence of ratio variation, in practice depends on the slope of the system which is low at shorter wavelengths and high at longer wavelengths which results in a larger error at shorter wavelengths than at longer wavelengths. In the example shown in Fig. 24 for a fiber filter of 10.5 mm radius and 15 turns it is estimated that the maximum wavelength error at 1500 nm is 1.9 nm from the original value. Any measured error in wavelength should be within this estimated wavelength error range.

From the figure it is clear that the measured ratio and wavelength variation of the system are well within the estimated limits. The effect of fluctuation in the attenuation due to PDL, which leads to the variation in ratio and measured wavelength, is confirmed by the results.
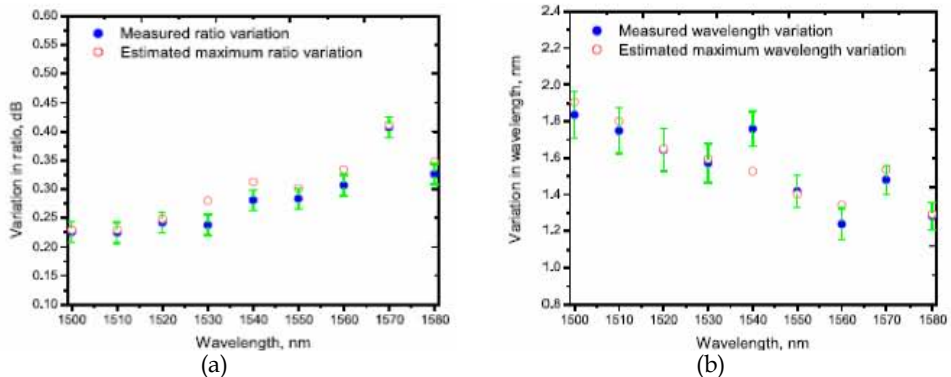

Fig. 24. Comparison of measured error with the estimated maximum error because of PDL (a) ratio error (b) wavelength error.

Without predicting the wavelength error due to PDL of the components used in the system, characterizing a system to a wavelength resolution or accuracy such as 0.01 nm is meaningless. Thus to determining the accuracy and resolution of the system, it is essential that the PDL and its effects on the system are quantified.

6. Polarization dependent loss minimization techniques

In the case of macro-bend fiber filter since the PDL of the filter originates from the difference in bend loss for TE and TM modes one method to compensate the bend loss of the modes is to split the fiber filter into two bending sections with equal length and introduce a 90^0 twist in the middle of the filter between the two sections (Rajan et al., 2008). This changes the polarization state for the second bending section, i.e., the TE (TM) mode is turned to be the TM (TE) mode

for the second bending section. The net effect is that the individual losses for the input TE and TM modes are equalized over the total length of the fiber so that the PDL can be minimized for the whole bending section. The schematic of the configuration is shown in Fig. 25.
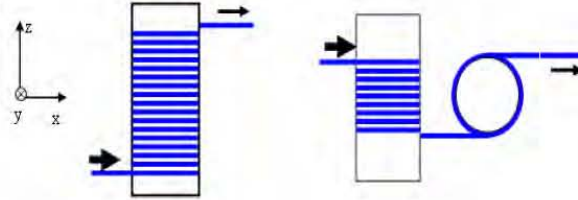

Fig. 25. Bending configurations of the macro-bend fiber filter: conventional bending and a 90^0 twist between the bending sections.

To demonstrate how the 90^0 twist reduces the PDL at higher bend lengths, the PDL of the filter is measured for different bend lengths and is shown in Fig. 26(a). For comparison the PDL of fiber filters without a twist is also presented for the same number of turns. From the figure it is clear that PDL is not eliminated completely in the fiber filter due to physical inaccuracies such as small variations in the bend length of the two sections of the filter and variations in the twist angle from 90^0 leading to residual PDL. It should be noted that a twist in the fiber induces circular birefringence and can make the fiber polarization dependent. However, such stress induced birefringence is very low in SMF28 fiber which means that the twist induced birefringence is negligible and its contribution to the PDL of the fiber filter is very small. Overall from the figures it is clear that the PDL of the fiber filter decreases considerably with a 90^0 twist at higher bend lengths which in turn allows the filter to utilize a larger number of turns to obtain the required steepness and thus increase the measurement resolution of the system without reaching an unacceptable level of PDL.

The PDL of an SMS structure can be reduced/eliminated by using accurate splicing methods which reduce the lateral offset between the SMF and the MMF at both ends. However conventional fusion splicers cannot guarantee a perfect splicing without lateral offset. In such cases by introducing a rotational offset of 90^0 will minimize the PDL as shown in Fig. 20. This is because at a rotational core offset of 90^0, the orientation between the input/output SMF and the input field direction of TE/TM are parallelized. Thus the overlap between the field profile at the output end of the MMF section and the eigen-mode profile of the output SMF for both TE and TM modes are similar and thus the PDL will be minimised.

Minimizing the polarization dependency of the fiber filter alone will not minimize the polarization dependency of the whole system. As the system contains another PDL component, the 3 dB coupler, it is important to minimize the PDL of the coupler also. One way to minimize the total polarization dependency of the system is using a polarization insensitive (PI) 3 dB couplers (couplers with very low PDL, in the range of 0.01 - 0.02 dB). The wavelength inaccuracy of a macro-bend fiber filter together with low PI 3 dB coupler and its comparison with conventional system are shown in Fig. 26(b). Thus, for wavelength measurements based on macro-bend fiber filters the polarization dependency can be significantly reduced by the 90^0 twisted fiber filter together with low PI 3 dB coupler

configuration and can deliver measurements with high wavelength accuracy irrespective of the input state of polarization.
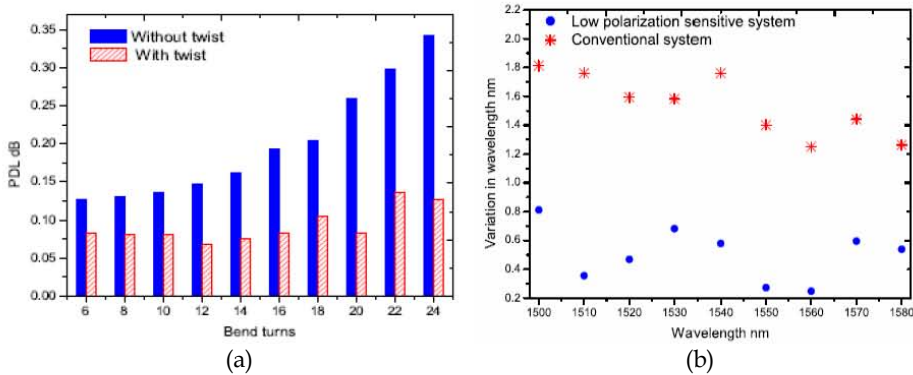

(a)   (b)

Fig. 26. (a) PDL of the fiber filters with 90^0 twist and its comparison with the PDL of the filters without twist (b) Comparison of wavelength errors in a low polarization system vs. conventional system

7. Temperature induced inaccuracies in a macro-bend fiber filter based WMS

When a single-mode fiber forms a macro-bend, WGMs may be created, which propagate in the cladding or buffer. These WGMs can interfere with the guided core mode to produce interference induced oscillations in the bend loss spectral response (Morgan et al., 1990). The dominant source of WGMs is the buffer-air interface and also the cladding-buffer interface. The formation of such whispering gallery modes effectively creates an interferometer within the fiber, with the core and buffer/cladding as the two arms. To utilize a macro-bend fiber as an edge filter, an absorption layer is applied to the buffer coating to eliminate these WG modes, which makes the bend loss spectral response smoother and ideally achieves a linear response versus wavelength as explained earlier.

The temperature sensitivity of such a fiber filter arises mainly from the temperature sensitive properties of the buffer coating, characterized by the thermo-optic coefficient (TOC) and thermal expansion coefficient (TEC). The TOC and TEC of the buffer coatings, such as acrylates, are much higher than those of fused silica which forms the core and the cladding of the fiber. Macro-bend fiber edge filters can be based on low bend loss fiber such as SMF28 fiber or high bend loss fiber such as 1060XP as explained in section 2.

The most common single-mode fiber, SMF28 fiber, has two buffer coating layers. Due to the coating layers, even with the absorption layer a low level of reflection from the cladding-primary coating boundary will still exist and interfere with the core mode. As a result of this when there is a change in temperature which changes the refractive index and thickness of the buffer coating, the path length variation of the WG modes and phase difference between the WG mode and the core mode leads to constructive and destructive interference between the WG mode and the core mode. This results in oscillatory variations in the spectral response of the bend loss. In a macro-bend fiber filter without a buffer coating but with an

applied absorption layer the temperature induced periodic variations in the bend loss can be eliminated.

A fiber filter based on SMF28 fiber requires multiple bend turns with small bend radii to achieve a better slope and high wavelength resolution. The removal of the buffer coating over a meter or more of fiber is beyond practical limits as the fiber breaks if it is wrapped for more than one turn at small bend radii without a buffer. However, a fiber such as 1060XP is highly sensitive to bend effects due its low normalized frequency (V). The V parameter for 1060XP fiber is 1.5035 while for SMF28 fiber it is 2.1611. Since the normalized frequency of the 1060XP is smaller, power will be less confined in the core and will be more susceptible to bending loss and the bend loss will be higher when compared to SMF28. As a result an edge filter based on a bend sensitive 1060XP fiber requires only one bend turn and hence the buffer can be stripped easily and an absorption layer can be applied directly to the cladding.

After removing the buffer coating from the sensor head, the only negative TOC material is eliminated and the sensor head consists of only positive TOC materials; the cladding and core, which are made of silica. For the silica core and cladding the thermally induced effective change in refractive index is linear in nature, resulting in a linear variation of bend loss with temperature. Since the temperature dependent loss is proportional to the bend loss in the fiber filter, 1060XP fiber shows higher temperature induced loss, when compared to its SMF28 counterpart, for the case of a single bend turn. For a system with this configuration, a temperature corrected calibration is feasible. A temperature corrected calibration means that temperature of the fiber filter is continually measured and therefore, the measurement system can apply correction factors to the calibration in use. This allows the system to be used over a wide range of ambient temperatures (Rajan et al., 2009).
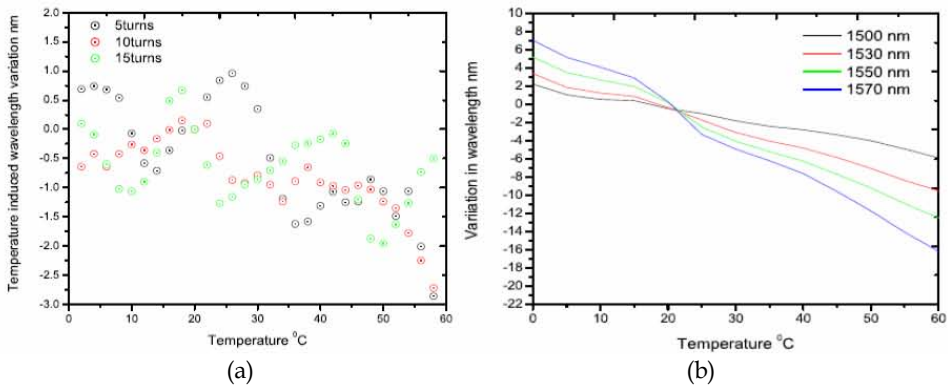

Fig. 27. Temperature induced wavelength error (a) SMF28 fiber filter (b) 1060XP fiber filter

A comparison of wavelength errors due to ambient temperature variation in the case of edge filters fabricated from standard singlemode fiber (SMF28) and bend sensitive fiber (1060XP) are shown in Fig. 27(a) and Fig. 27(b) respectively. While it is apparent that the SMF28 fiber filter based system is less temperature sensitive, nevertheless the oscillatory nature of the bend loss and ratio of the system makes correction of the calibrated response unfeasible. For the SMF28 based filter the only option is to use active temperature stabilization of the filter

temperature. Whereas for the bend sensitive fiber based filter temperature compensation requires a sensor and compact electronics only, temperature stabilization will additionally demand a Peltier cooler, heat sinks, a complex feedback control system and, depending on the ambient temperature variation to be dealt with, will involve significantly higher power consumption by the system.

The temperature stabilization approach will thus require more physical space, as well as higher complexity and cost than the temperature compensation approach. Using high bend loss fibers such as 1060XP will mean that the fiber filter will have higher temperature dependence than the SMF28 fiber filter, but due to the linear nature of the ratio variation with temperature, the temperature induced error can be compensated by adding correction factors to the calibration ratio response. The wavelength accuracy can be improved by obtaining the correction in the ratio response with smaller temperature intervals or by extrapolating the correction response between the required temperature intervals. Thus, irrespective of the temperature dependence of the 1060XP fiber filter, such a filter can be operated over a wide temperature range, if the correction in ratio response is added to the original ratio response and thus precise wavelength measurements can be obtained.

8. Summary

A brief review of all-fiber passive edge filters for wavelength measurements is presented in this chapter. Along with the review two recently developed fiber edge filters: a macro-bend fiber filter and a singlemode-multimode-singlemode fiber edge filter are also presented. For the macro-bend fiber filter an optimization of the bend radius and the number of bend turns together with the application of an absorption coating is required in order to achieve a desired edge filter spectral response. For the SMS fiber filter, the length of the MMF section sandwiched between the singlemode fibers is important. The length of the MMF section determines the operating wavelength range of the filter.

The main factors that affect the performance accuracy of edge filter based ratiometric wavelength measurement are also discussed in this chapter. Due to the limited SNR of the optical source and the noise in the receiver system, the measurable wavelength range is limited and also it is not possible to achieve a uniform resolution throughout the wavelength range. The resolution of the system depends on the filter slope and the noise in the system.

The origin of the polarization sensitivity of the components of a ratiometric system is also analysed in this chapter. The polarization sensitivity of a 3 dB coupler, a macro-bend fiber filter and a SMS fiber filter are explained. Since a ratiometric wavelength measurement system consists of more than one PDL component, the net PDL depends on the relative orientation of the PDL axes of each component. A theoretical model to predict the ratio and wavelength fluctuation due to the polarization dependence of the components involved in the system is presented. It is concluded that for determining the accuracy and resolution of the system the PDL of the system and its effects on the system performance have to be quantified. To minimize the effect of PDL on a macro-bend and a SMS fiber filters, methods to minimize the polarization dependence are also presented. In the case of a macro-bend fiber filter, PDL can be minimized by dividing the filter into two sections and by introducing

a 90^0 twist between the two bending sections. For SMS fiber filters PDL can be minimized by reducing the lateral core offset and also by introducing a 90^0 rotational offset.

The influence of temperature on a macro-bend fiber based wavelength measurement system is also presented in this chapter. The temperature dependencies of two types of macro-bend fiber filters based on SMF28 and 1060XP fibers are presented. In the case of SMF28 fiber based filter, the temperature dependence is lower, but the response is oscillatory in nature, which makes correction to the temperature calibration too complex to be feasible. In the case of 1060XP fiber based system, the temperature dependence is higher but since it is linear in nature a temperature correction to the calibration response is feasible.

9. References

Davis, M. A. & Kersey, A. D. (1994). All-fiber Bragg grating strain sensor demodulation technique using a wavelength division coupler, *Electron. Lett.*, 30, 75–77

El Amari, A.; Gisin, N.; Perny, B.; Zbinden, H. & Zimmer, W. (1998). Statistical prediction and experimental verification of concatenations of fiber optic components with polarization dependent loss, *IEEE J. Lightwave Technol.*, 16, 332–339

Fallon, R. W.; Zhang, L.; Everall, L. A. & Williams, J. A. R. (1998). All fiber optical sensing system: Bragg grating sensor interrogated by a long period grating, *Meas. Sci. Technol.*, 9, 1969–1973

Fallon, R. W.; Zhang, L.; Gloang, A. & Bennion, I. (1999). Fabricating fiber edge filters with arbitrary spectral response based on tilted chirped grating structures, *Meas. Sci. Technol.*, 10, L1–L3

Gisin, N. (1995). The statistics of polarization dependent losses, *Optics Communications*, 114, 399–405

Hill, K. O. & Meltz, G. (1997). Fiber Bragg grating technology fundamentals and overview, IEEE *J. Lightwave Technol.*, 15, 1263–1276

Kersey, A. D.; Berkoff, T. A. & Morey, W. W. (1992). High resolution fiber grating sensor with interferometric wavelength shift detection, *Electron. Lett.*, 28, 236–138

Kersey, A. D.; Berkoff, T. A. & Morey, W. W. (1993). Multiplexed fibre Bragg grating strain-sensor system with a fibre Fabry Perot wavelength filter, *Opt. Lett.*, 18, 1370–1372

Mille, S. M.; Liu, K. & Measures, R. M. (1992). A passive wavelength demodulation system for guided wave Bragg grating sensors, *IEEE Photon. Tech Lett.*, 4, 516–518

Morgan, R.; Barton, J. S.; Harper, P. G. & Jones, J. D. C. (1990) Temperature dependence of bending loss in monomode optical fibers, *Electron. Lett.*, 26, 937–939

Motechenbacher, C. D. & Connelly, J. A. (1993). *Low-Noise Electronic System Design*, John Wiley and Sons, Inc

Mourant, J. R.; Bigio, I. J.; Jack, D. A.; Johnson, T. M. & Miller, H. D. (1997). Measuring absorption coefficients in small volumes of highly scattering media: source-detector separations for which path lengths do not depend on scattering properties, *Appl. Opt.*, 36, 5655–5661

Rajan, G.; Wang, Q.; Farrell, G.; Semenova, Y. & Wang, P. (2007). Effect of SNR of input signal on the accuracy of a ratiometric wavelength measurement system, *Microwave and Optical Technology Letters*, 49, 1022–1024

Rajan, G.; Semenova, Y.; Freir, T.; Wang, P. & Farrell, G. (2008). Modeling and analysis of the effect of noise on an edge filter based ratiometric wavelength measurement system, *IEEE J. Lightwave Technol.*, 26, 3434-3442

Rajan, G.; Wang, Q.; Semenova, Y.; Farrell, G. & Wang, P. (2008). Effect of polarization dependent loss on the performance accuracy of a ratiometric wavelength measurement system, *IET Optoelectron.*, 2, 63–68

Rajan, G.; Semenova, Y.; Farrell, G.; Wang, Q. & Wang, P. (2008). A low polarization sensitivity all-fiber wavelength measurement system, *IEEE Photon. Technol. Lett.*, 20, 1464–1466

Rajan, G.; Semenova, Y.; Wang, P. & Farrell, G. (2009). Temperature induced instabilities in macro-bend fiber based wavelength measurement systems, *IEEE J. Lightwave Technol.*, 27, 1355-1361

Ribeiro, A. B. L.; Ferreira, L. A.; Tsvetkov, M. & Santos, J. L. (1996). All fiber interrogation technique for fiber Bragg sensors using a biconical fiber filter, *Electron. Lett.*, 32, 382–383

Wang, Q.; Farrell, G. & Freir, T. (2005). Theoretical and experimental investigations of macro bend losses for standard single mode fibers, *Optics Express*, 13, 4476–4484

Wang, Q. & Farrell, G. (2006). Multimode fiber based edge filter for optical measurement and its design, Microwave and Optical Technology Letters, 48, 900–902

Wang, Q.; Farrell, G.; Freir, T.; Rajan, G. & Wang, P. (2006). Low cost wavelength measurement based on macrobending singlemode fiber, *Opt. Lett.*, 31, 1785–1787

Wang, Q.; Rajan, G.; Wang, P. & Farrell, G. (2007). Polarization dependence of bend loss in a standard singlemode fiber, *Optics Express*, 1, 4909–4920

Wang, P.; Farrell, G.; Wang, Q. & Rajan, G. (2007). An optimized macrobending fiber-based edge filter, *IEEE Photon. Technol. Lett.*, 19, 1136–1138

Wang, Q.; Farrell, G. & Yan, W. (2008). Investigation on singlemode- multimode- singlemode fiber structure, *IEEE J. Lightwave Technol.*, 26, 512–519

Zhao, Y & Liao, Y. (2004). Discrimination methods and demodulation techniques for fiber Bragg grating sensors, *Optics and Lasers in Engg.*, 41, 1–18

Wu, T. L. & Chang, H. C. (1995). Rigorous analysis of form birefringence of weakly fused fiber-optic couplers, *IEEE J. Lightwave Technol.*, 13, 687– 691

Wu, T. L. (1999). Vectorial analysis for polarization effect of wavelength flattened fiber-optic couplers, *Microwave and Optical Technology Letters*, 23, 12–16

Xu, M. G.; Geiger, H. & Dakin, J. P. (1996). Modeling and performance analysis of a fiber Bragg grating interrogation system using an acousto-optic tunable filter, *IEEE J. Lightwave Technol.*, 14, 391-396